

# Semantic Class Distribution Learning for Debiasing Semi-Supervised Medical Image Segmentation

Yingxue Su<sup>1</sup>, Yiheng Zhong<sup>†1</sup>, Keying Zhu<sup>1</sup>, Zimu Zhang<sup>1</sup>, Zhuoru Zhang<sup>1</sup>,  
Yifang Wang<sup>2</sup>, YuXin Zhang<sup>3</sup>, and Jingxin Liu<sup>†1</sup>

<sup>1</sup> Xi'an Jiaotong-Liverpool University, Suzhou, China

<sup>2</sup> University College London, London, United Kingdom

<sup>3</sup> Wuhan University, Wuhan, China

JohnZhongJohn@outlook.com

**Abstract.** Medical image segmentation is critical for computer-aided diagnosis. However, dense pixel-level annotation is time-consuming and expensive, and medical datasets often exhibit severe class imbalance. Such imbalance causes minority structures to be overwhelmed by dominant classes in feature representations, hindering the learning of discriminative features and making reliable segmentation particularly challenging. To address this, we propose the Semantic Class Distribution Learning (SCDL) framework, a plug-and-play module that mitigates supervision and representation biases by learning structured class-conditional feature distributions. SCDL integrates Class Distribution Bidirectional Alignment (CDBA) to align embeddings with learnable class proxies and leverages Semantic Anchor Constraints (SAC) to guide proxies using labeled data. Experiments on the Synapse and AMOS datasets demonstrate that SCDL significantly improves segmentation performance across both overall and class-level metrics, with particularly strong gains on minority classes, achieving state-of-the-art results. Our code is released at <https://github.com/Zyh5555/SCDL>.

**Keywords:** Semi-Supervised Learning · Proxy Learning · Feature Alignment · Medical Image Segmentation · Class Imbalance

## 1 Introduction

Accurate and reliable medical image segmentation is crucial for computer-aided diagnosis. However, dense pixel-level annotation is both time-consuming and expensive[27,3,13,21]. Therefore, Semi-Supervised Medical Image Segmentation (SSMIS) has attracted widespread attention, as it typically leverages unlabeled data to alleviate annotation burden through strategies such as consistent regularization and contrastive representation learning[1,27,17,10,16]. However, in real-world scenarios, medical segmentation often suffers from class imbalance.

---

<sup>†</sup>Corresponding author.

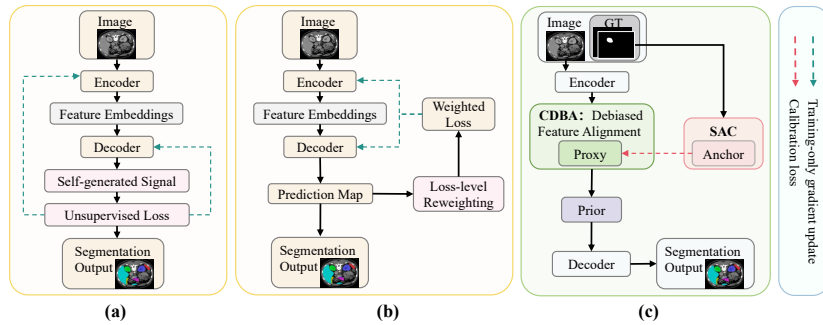


Fig. 1: Comparison of imbalance-aware SSMIS paradigms: (a) Self-generated supervision uses model-derived unlabeled signals and may amplify head-class bias. (b) Loss reweighting and output calibration rebalance training but do not constrain class-conditional features. (c) SCDL debiases feature distributions via CDDBA, distribution priors, and SAC anchoring.

This imbalance causes the training process to be dominated by large structures. Under conditions of scarce annotations, small structures are difficult to segment in a stable and reliable manner[15,27,28,25].

Under such a pixel-level long-tailed distribution, the combination of class imbalance and semi-supervised mechanisms gives rise to two major challenges. As shown in Fig. 1, the first supervision signal becomes systematically biased toward head classes. Since large organs occupy more pixels, the model’s gradient updates are more likely to favor these classes. Many SSMIS methods rely on self-generated signals from unlabeled data, such as soft pseudo labeling and consistency constraints, which further reinforce the learning of head classes and result in insufficient training for tail classes [15,27,11]. Second, this bias leads to an imbalance at the representation level. Existing methods often mitigate imbalance through techniques such as reweighting or output alignment, but these approaches mainly operate at the loss or output level and lack direct constraints on class-conditional feature distributions [9,18,7,4]. As a result, features of head classes become more compact, while features of tail classes drift toward regions dominated by head classes, which blurs class boundaries and degrades segmentation performance on small structures [20,28,19]. Notably, many existing methods use unlabeled data mainly for local consistency regularization and rarely exploit it to explicitly correct the skewness of class-conditional feature distributions [24,18,26,8]. Therefore, unlabeled data does not promote well-structured feature representations for minority classes, allowing the existing imbalance to persist.

To address the above limitations, we propose a Semantic Class Distribution Learning (SCDL) framework, as illustrated in Fig. 2. The framework is integrated into existing segmentation networks as a plug-and-play module. While fully leveraging labeled data to provide semantic supervision, it guides unlabeled data to participate in learning at the distribution level, thereby learning structured class-conditional feature distributions in the embedding space. This

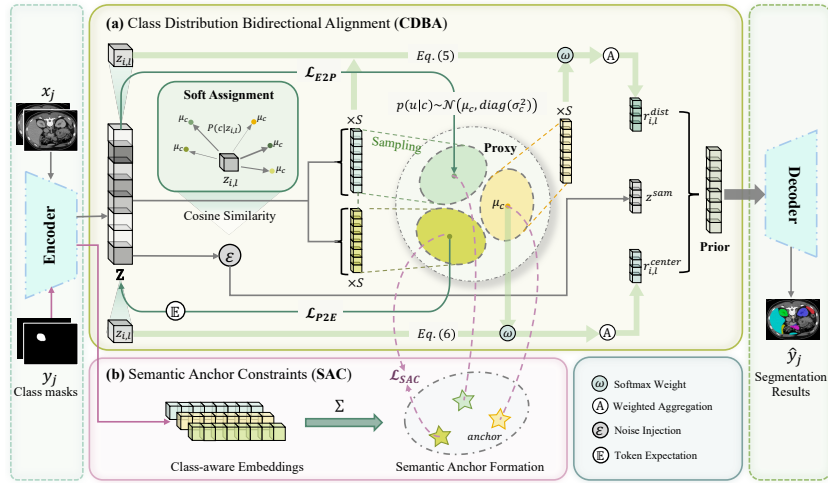


Fig. 2: **Overview of SCDL.** (a) **CDBA** learns class proxy distributions and aligns them with token features to generate proxy-guided priors for downstream tasks. (b) **SAC** extracts semantic anchors from labeled regions and uses them to regularize the proxies, ensuring consistent class semantics across categories.

explicitly reshapes the class-conditional feature structure and mitigates both supervision bias and representation-level imbalance. Class Distribution Bidirectional Alignment (CDBA) models each semantic class as a learnable proxy distribution and enforces bidirectional alignment constraints between embeddings and the proxy distributions. This mechanism is not affected by differences in sample scale across classes and enables stable modeling of minority class distributions while providing consistent learning signals. Semantic Anchor Constraints (SAC) align each proxy distribution with semantic anchors constructed from labeled data, providing reliable semantic supervision to ensure that the proxy distributions capture the true semantics of each class. This process refines the supervision signal, corrects learned representations, and prevents bias from class frequency imbalance, thereby ensuring consistency feature representations.

Our contributions are summarized as follows: (i) We propose the SCDL framework, which mitigates supervision bias and representation-level imbalance by learning structured class-conditional distributions. (ii) We introduce CDBA, which shapes class-conditional structures through bidirectional alignment between embeddings and proxy distributions. (iii) We propose SAC, which uses labeled data to construct semantic anchors, guiding proxy distributions toward true class semantics. (iv) Experiments on the Synapse and AMOS datasets show that SCDL achieves state-of-the-art results in overall and tail-class segmentation.

## 2 Methodology

### 2.1 Class Distribution Bidirectional Alignment (CDBA)

To mitigate supervision and representation bias toward head classes, CDBA learns structured class-conditional distributions in the embedding space and enforces bidirectional alignment between embeddings and distributions, enabling minority classes to receive consistent supervision even under sparse annotations.

**Class Distribution Modeling.** Each semantic class  $c \in \{1, \dots, C\}$  is represented by a learnable proxy distribution in the embedding space:

$$p(u|c) = \mathcal{N}(\mu_c, \text{diag}(\sigma_c^2)), \quad (1)$$

where  $\mu_c$  denotes the mean vector of class  $c$ , and  $\sigma_c$  denotes the standard deviation vector for each dimension; the corresponding diagonal covariance matrix is  $\text{diag}(\sigma_c^2)$ ; both  $\mu_c$  and  $\sigma_c$  are randomly initialized and parameterized as trainable proxies. Given a batch of embeddings  $\mathbf{Z} \in \mathbb{R}^{B \times L \times D}$ , we compute a soft assignment of each token embedding to all class proxies:

$$P(c|z_{i,l}) = \text{softmax}_c(\cos(z_{i,l}, \mu_c)), \quad (2)$$

where  $z_{i,l} \in \mathbb{R}^D$  denotes the  $l$ -th token embedding of the  $i$ -th sample in the mini-batch, and  $\cos(\cdot, \cdot)$  is the cosine similarity. This soft assignment enables each embedding to associate with multiple classes, alleviating supervision bias and allowing gradients to flow to minority-class proxies even under sparse labels. To further prevent minority-class embeddings from being dominated by majority distributions, we introduce bidirectional distribution alignment to explicitly align embeddings with their corresponding class distributions:

**(i) Embedding-to-Proxy (E2P) Alignment** Each embedding is encouraged to move closer to its soft-assigned proxy distributions:

$$\mathcal{L}_{E2P} = \sum_{i=1}^B \sum_{l=1}^L \sum_{c=1}^C P(c|z_{i,l}) \cdot [1 - \cos(z_{i,l}, \mu_c)]. \quad (3)$$

By weighting cosine distance with soft assignment probabilities,  $\mathcal{L}_{E2P}$  encourages embeddings to align with class proxies. This soft weighting allows each embedding to influence multiple proxies according to its assignment weights, promoting balanced gradient flow and mitigating majority-class dominance.

**(ii) Proxy-to-Embedding (P2E) Alignment.** Each proxy is optimized to discriminate its softly assigned embeddings. The P2E loss is defined as:

$$\mathcal{L}_{P2E} = \frac{1}{C} \sum_{c=1}^C \exp\left(-(\mathcal{E}_c^+ - \mathcal{E}_c^-)\right), \quad (4)$$

$$\mathcal{E}_c^+ - \mathcal{E}_c^- = \mathbb{E}_{i,l} \left[ (2P(c|z_{i,l}) - 1) \cos(z_{i,l}, \mu_c) \right].$$

The operator  $\mathbb{E}_{i,l}[\cdot]$  denotes the expectation over all tokens in the current mini-batch. This objective encourages each proxy to achieve higher similarity with

embeddings assigned to its class while maintaining lower similarity with embeddings from other classes, thereby enhancing proxy discriminability.

**Proxy Sampling and Feature Enrichment.** To leverage the learned class-conditional proxy distributions for structured semantic guidance, we construct token-wise embedding priors via lightweight proxy sampling, enabling more robust estimation of token-to-class similarities under distributional uncertainty.

**(i) Distribution-Weighted Prior.** For each embedding  $z_{i,l}$ , we construct a weighted combination of proxy means  $\mu_c$ , where the weights are computed from  $S$  samples drawn from the proxy distributions, reflecting distribution similarity:

$$\mathbf{r}_{i,l}^{dist} = \sum_{c=1}^C \frac{\exp\left(\frac{1}{S} \sum_{s=1}^S \cos(z_{i,l}, u_c^s)\right)}{\sum_{c'=1}^C \exp\left(\frac{1}{S} \sum_{s=1}^S \cos(z_{i,l}, u_{c'}^s)\right)} \mu_c \in \mathbb{R}^D. \quad (5)$$

where  $u_c^s \sim \mathcal{N}(\mu_c, \text{diag}(\sigma_c^2))$  denotes the  $s$ -th sample drawn from the proxy distribution of class  $c$ . This prior captures distribution-level structure, including variance, while preserving soft multi-class associations, injecting structured semantic information into each token representation.

**(ii) Center-Similarity Prior.** In contrast, the center-similarity prior aligns each token directly to the class means:

$$\mathbf{r}_{i,l}^{center} = \sum_{c=1}^C \frac{\exp(\cos(z_{i,l}, \mu_c))}{\sum_{c'=1}^C \exp(\cos(z_{i,l}, \mu_{c'}))} \mu_c \in \mathbb{R}^D. \quad (6)$$

Unlike the distribution-weighted prior, this mean-based reweighting ignores variance but provides complementary token-to-class signals, improving representation stability and discriminability. Additionally, we perform local perturbation sampling around each token with a learnable noise scale, aggregating normalized samples to obtain a token sampling prior  $\mathbf{z}^{sam} \in \mathbb{R}^{B \times L \times D}$ , which enhances robustness. Finally, the three priors are concatenated along the feature dimension:

$$\mathbf{z}^{prior} = \text{concat}(\mathbf{r}^{dist}, \mathbf{r}^{center}, \mathbf{z}^{sam}), \quad (7)$$

A lightweight projection matches the decoder channel size, and the prior is re-sized for additive injection at each decoder stage, ensuring both head and tail classes contribute effectively to segmentation.

## 2.2 Semantic Anchor Constraints (SAC)

Although CDBA learns class-conditional distributions and enforces bidirectional alignment between embeddings and proxies, the proxies are randomly initialized and lack direct semantic supervision, leaving their correspondence to true class semantics unconstrained. To address this issue, we introduce Semantic Anchor Constraints (SAC), which provide high-level semantic guidance for proxy learning. SAC assumes that encoder embeddings from labeled regions contain sufficient class-specific semantic information. These embeddings are therefore

used to guide the learning of corresponding class proxies, promoting intra-class alignment and enhancing inter-class separability.

**Semantic Anchor Formation.** For each class, we identify class-specific regions based on ground-truth masks and mask out all non-target pixels. The masked class-specific images are passed through the encoder shared with the original image to obtain class-aware embeddings.

Formally, let  $\mathcal{Z}_c = \{z_{i,l} \mid (x_i, y_i) \in \mathcal{D}_L, \tilde{m}_{i,l}^{(c)} = 1\}$  denote the set of class-aware embeddings for class  $c$ , where  $\tilde{m}_{i,l}^{(c)}$  indicates whether the region corresponding to embedding  $z_{i,l}$  belongs to class  $c$ , then the semantic anchor is computed as

$$\text{anchor}_c = \frac{1}{|\mathcal{Z}_c|} \sum_{z \in \mathcal{Z}_c} z. \quad (8)$$

During backpropagation, semantic anchors are detached to prevent gradients from updating the encoder, ensuring that the SAC loss only updates the proxy.

**Semantic Anchor Alignment.** Each class proxy  $\mu_c$  is aligned with its corresponding semantic anchor using a cosine similarity-based loss:

$$\mathcal{L}_{\text{SAC}} = \frac{1}{C} \sum_{c=1}^C [1 - \cos(\mu_c, \text{anchor}_c)]. \quad (9)$$

This constraint guides proxies to encode class-specific semantic information while maintaining consistency across classes, including those with few samples.

## 3 Experiment

### 3.1 Dataset and Implementation Details

We evaluate our method on two multi-organ CT datasets, Synapse[6] and AMOS[5]. The Synapse dataset consists of 30 CT scans with 13 organ categories. The foreground classes include the spleen(Sp), right and left kidneys(RK, LK), gallbladder(Ga), esophagus(Es), liver(Li), stomach(St), aorta(Ao), inferior vena cava(IVC), portal and splenic veins(PSV), pancreas(PA), and right and left adrenal glands (RAG, LAG). Following the split used in DHC[22] and GA[14], 20 scans are used for training, 4 for validation, and 6 for testing. The AMOS dataset comprises 360 subjects and 15 organ categories. Building upon Synapse, AMOS introduces three additional classes, prostate/uterus(P/U), duodenum(Du), and bladder(BI), while excluding the portal and splenic veins (PSV). The dataset is split into 216 scans for training, 24 for validation, and 120 for testing. All experiments are conducted on an NVIDIA A40 GPU. The batch size is set to 4 for all experiments. The weight decay for the SCDL module is set to 1e-4. All other training configurations follow the corresponding baseline settings [23,22,14]. We report the Dice Similarity Coefficient (DSC,%) and Average Surface Distance (ASD) for evaluation, where higher DSC and lower ASD indicate better performance.

Table 1: Comparison of quantitative results with state-of-the-art models on Synapse (20% labeled) and AMOS (5% labeled).

Methods	Synapse (20% labeled)		AMOS (5% labeled)	
	DSC↑	ASD↓	DSC↑	ASD↓
VNet (fully)[12]	68.49±3.5	6.08±5.4	76.50±2.1	2.01±3.2
GenericSSL [23]	55.94±3.5	6.14±1.7	35.73±2.3	45.82±1.2
SimiS [2]	50.45±2.7	33.11±3.6	47.27±1.6	11.51±2.3
CLD [9]	49.47±2.9	34.73±7.6	46.10±2.5	15.86±4.3
DHC [22]	46.16±2.4	10.04±0.8	40.11±2.3	40.65±1.1
A&D [23]	60.88±0.7	<b>2.52±0.4</b>	37.82±1.1	44.31±0.8
GA-MagicNet [14]	66.00±1.9	3.42±0.6	59.15±1.5	8.66±1.3
GA-CPS [14]	66.29±0.3	5.44±0.4	50.90±0.5	13.77±0.6
<b>SCDL-GenericSSL</b>	58.90±0.9	5.79±0.5	47.35±1.0	22.84±0.9
<b>SCDL-DHC</b>	49.17±2.3	10.59±0.5	49.28±2.1	17.47±0.6
<b>SCDL-GA-MagicNet</b>	66.75±1.3	3.65±0.3	<b>62.16±1.2</b>	<b>5.65±0.4</b>
<b>SCDL-GA-CPS</b>	<b>67.50±0.9</b>	3.32±0.8	61.57±1.0	10.08±1.1

Table 2: Per-class Dice scores (%) on the Synapse dataset with 20% labeled data.

Methods	Average Dice of Each Class													
	Sp	RK	LK	Ga	Es	Li	St	Ao	IVC	PSV	PA	RAG	LAG	
VNet (fully)[12]	90.2	91.9	90.7	38.3	30.9	94.8	75.6	79.1	81.4	62.1	48.5	48.9	58.0	
GenericSSL [23]	86.3	77.9	83.8	16.1	28.2	87.0	37.9	75.2	70.4	43.4	39.4	40.4	41.4	
SimiS [2]	83.3	90.8	85.8	9.2	0.0	85.6	55.0	73.6	71.7	50.4	34.0	0.0	16.6	
CLD [9]	83.3	86.7	85.7	1.3	0.0	85.9	49.1	74.5	76.3	52.4	33.8	14.1	0.0	
DHC [22]	65.4	82.3	74.7	17.9	14.7	75.1	22.7	64.2	58.0	30.7	25.9	27.9	40.5	
A&D [23]	85.2	66.9	67.0	<b>52.7</b>	<b>62.9</b>	89.6	52.1	<b>83.0</b>	74.9	41.8	43.4	44.8	27.2	
GA-MagicNet [14]	79.4	<b>92.2</b>	89.5	24.0	48.1	90.7	52.9	80.7	81.2	64.6	43.3	48.5	<b>62.9</b>	
GA-CPS [14]	85.5	90.1	88.3	26.7	40.2	92.7	<b>64.8</b>	79.7	79.1	<b>66.8</b>	45.5	44.7	57.4	
<b>SCDL-GenericSSL</b>	86.2	83.4	83.1	16.4	33.8	87.6	46.2	76.1	72.7	49.9	43.0	42.4	45.1	
<b>SCDL-DHC</b>	64.9	82.4	77.5	9.6	23.5	78.0	28.3	65.3	67.6	42.6	27.5	36.7	35.4	
<b>SCDL-GA-MagicNet</b>	79.3	91.5	<b>90.3</b>	20.3	49.8	88.9	63.5	79.0	80.8	64.6	46.5	<b>51.6</b>	61.6	
<b>SCDL-GA-CPS</b>	<b>88.2</b>	91.7	89.3	25.4	38.7	<b>93.7</b>	64.4	78.0	<b>81.8</b>	65.4	<b>49.4</b>	49.2	62.4	

### 3.2 Comparisons with State-of-the-art Methods

We compare SCDL with representative semi-supervised methods for class imbalance. As summarized in Table 1, integrating SCDL consistently increases mean DSC and decreases ASD on both Synapse (20% annotations) and AMOS (5% annotations). On Synapse, SCDL-DHC outperforms DHC baseline by +3.01% in mean DSC, showing the most pronounced overlap improvement. Meanwhile, SCDL decreases ASD by -2.12 compared with the GA-CPS baseline. On AMOS, the improvements are more pronounced, with mean DSC gains up to +11.62% achieved by SCDL-GenericSSL, and a substantial ASD reduction on DHC, where SCDL decreases ASD from 40.65 to 17.47(↓ 23.18), indicating that boundary errors can be substantially reduced even under extremely limited annotations.

Table 2 and Table 3 further report the per-class Dice scores on Synapse and AMOS, respectively. The gains are mainly concentrated on long-tailed, small-organ categories. On Synapse, SCDL-DHC notably improves segmentation on

Table 3: Per-class Dice scores (%) on the AMOS dataset with 5% labeled data.

Methods	Average Dice of Each Class														
	Sp	RK	LK	Ga	Es	Li	St	Ao	IVC	PA	RAG	LAG	Du	Bl	P/U
VNet (fully) [12]	92.2	92.2	93.3	65.5	70.3	95.3	82.4	91.4	85.0	74.9	58.6	58.1	65.6	64.4	58.3
GenericSSL [23]	58.9	67.5	70.4	15.5	0.0	73.8	46.6	57.2	49.6	41.1	0.0	0.0	24.5	30.6	0.2
SimiS [2]	77.4	72.5	68.7	32.1	14.7	86.6	46.3	74.6	54.2	41.6	24.4	17.9	21.9	47.9	28.2
CLD [9]	67.2	68.5	71.4	41.0	21.0	76.1	42.4	69.8	52.1	37.9	24.7	23.4	22.7	38.1	35.2
DHC [22]	65.9	65.1	70.2	0.1	4.8	76.8	50.5	75.8	56.8	50.0	0.0	0.0	26.1	46.1	14.4
A&D [23]	72.8	67.5	64.4	14.6	0.0	82.3	44.6	70.7	51.9	38.1	0.0	0.0	23.7	36.7	0.2
GA-MagicNet [14]	80.3	82.0	80.0	46.1	43.1	<b>88.6</b>	50.9	79.8	64.4	52.4	42.9	34.2	31.0	<b>68.2</b>	43.1
GA-CPS [14]	71.3	62.0	59.0	35.2	38.2	76.1	50.7	62.2	58.8	43.9	44.0	28.8	29.0	62.6	41.6
<b>SCDL-GenericSSL</b>	74.0	79.5	78.9	30.6	44.8	84.0	50.3	75.3	62.3	45.5	0.0	20.3	27.6	36.9	0.2
<b>SCDL-DHC</b>	73.5	65.5	67.9	42.5	31.0	75.5	34.2	78.2	56.0	52.7	33.9	30.3	33.2	51.7	13.1
<b>SCDL-GA-MagicNet</b>	79.7	<b>84.0</b>	<b>84.4</b>	<b>50.0</b>	<b>50.6</b>	86.8	55.0	<b>84.6</b>	<b>70.9</b>	55.6	<b>46.3</b>	<b>40.0</b>	33.1	65.6	46.3
<b>SCDL-GA-CPS</b>	<b>81.7</b>	80.7	82.3	46.4	53.1	87.0	<b>63.0</b>	80.7	65.4	<b>56.8</b>	39.1	35.2	<b>39.1</b>	66.8	<b>46.4</b>

small organs, including portal and splenic veins ( $\uparrow$  11.9%), esophagus ( $\uparrow$  8.8%), and right adrenal gland ( $\uparrow$  8.8%). On AMOS, the Dice scores of the right and left adrenal glands increase from 0% to 33.9% and 30.3%, respectively, demonstrating effective recovery of severely under-represented classes. Overall, these results indicate that SCDL consistently enhances segmentation performance, with particularly strong benefits for tail classes.

### 3.3 Ablation Study

Table 4: Ablation study on the Synapse dataset.

#	baseline	CDBA	SAC	DSC $\uparrow$	ASD $\downarrow$
1	✓			66.29	5.44
2	✓	✓		66.77	6.24
3	✓	✓	✓	<b>67.50</b>	<b>3.32</b>

To validate the effectiveness of the two core components in SCDL, we conduct an ablation study on Synapse using 20% labeled data, as shown in Table 4. The baseline achieves 66.29% mean Dice and 5.44 ASD. Adding CDBA introduces class-conditional distributional constraints that improve region-level prediction consistency, leading to a +0.48% gain in mean Dice. However, ASD increases by +0.80, indicating that distribution-level alignment alone does not reliably improve boundary geometry. After further incorporating SAC, the full model attains the best performance with 67.50% mean Dice (+0.73% over CDBA) and a markedly reduced ASD of 3.32 ( $\downarrow$  2.92). These results suggest that semantic constraints from labeled regions enhance the stability and semantic consistency of proxies, thereby improving geometric boundary quality more reliably.

## 4 Conclusion

Semi-supervised methods often struggle with pixel-level long-tailed imbalance, where dominant large structures and pseudo-labeling with consistency regularization bias learning, destabilizing small-structure segmentation and blurring class boundaries. We propose SCDL, a class distribution debiasing framework for semi-supervised medical segmentation. It first uses bidirectional alignment to stabilize minority-class proxies, then semantic anchoring refines them toward labeled centers, preventing drift to majority classes. Across multiple datasets, SCDL consistently yields more balanced solutions with improved boundary precision on anatomically scarce regions.

## References

1. Chen, D., Bai, Y., Shen, W., Li, Q., Yu, L., Wang, Y.: Magicnet: Semi-supervised multi-organ segmentation via magic-cube partition and recovery. In: Proceedings of the IEEE/CVF Conference on Computer Vision and Pattern Recognition. pp. 23869–23878 (2023)
2. Chen, H., Fan, Y., Wang, Y., Wang, J., Schiele, B., Xie, X., Savvides, M., Raj, B.: An embarrassingly simple baseline for imbalanced semi-supervised learning. arXiv preprint arXiv:2211.11086 (2022)
3. Chen, J., Mei, J., Li, X., Lu, Y., Yu, Q., Wei, Q., Luo, X., Xie, Y., Adeli, E., Wang, Y., et al.: Transunet: Rethinking the u-net architecture design for medical image segmentation through the lens of transformers. *Medical Image Analysis* **97**, 103280 (2024)
4. Dong-DongChen, W., WeiGao, Z.: Tri-net for semi-supervised deep learning. In: Proceedings of the Twenty-Seventh International Joint Conference on Artificial Intelligence. pp. 2014–2020 (2018)
5. Ji, Y., Bai, H., Ge, C., Yang, J., Zhu, Y., Zhang, R., Li, Z., Zhanng, L., Ma, W., Wan, X., et al.: Amos: A large-scale abdominal multi-organ benchmark for versatile medical image segmentation. *Advances in neural information processing systems* **35**, 36722–36732 (2022)
6. Landman, B., Xu, Z., Iglesias, J.E., Styner, M., Langerak, T.R., Klein, A.: 2015 MICCAI multi-atlas labeling beyond the cranial vault workshop and challenge. In: Proc. MICCAI Multi-Atlas Labeling Beyond the Cranial Vault – Workshop Challenge. Springer (2015)
7. Lee, D.H., et al.: Pseudo-label: The simple and efficient semi-supervised learning method for deep neural networks. In: Workshop on Challenges in Representation Learning, ICML. vol. 3, p. 896. Atlanta (2013)
8. Li, Y., Chen, J., Xie, X., Ma, K., Zheng, Y.: Self-loop uncertainty: A novel pseudo-label for semi-supervised medical image segmentation. In: International Conference on Medical Image Computing and Computer-Assisted Intervention. pp. 614–623. Springer (2020)
9. Lin, Y., Yao, H., Li, Z., Zheng, G., Li, X.: Calibrating label distribution for class-imbalanced barely-supervised knee segmentation. In: International Conference on Medical Image Computing and Computer-Assisted Intervention. pp. 109–118. Springer (2022)

10. Liu, W., Tian, T., Xu, W., Yang, H., Pan, X., Yan, S., Wang, L.: Phtrans: Parallely aggregating global and local representations for medical image segmentation. In: International Conference on Medical Image Computing and Computer-Assisted Intervention. pp. 235–244. Springer (2022)
11. Lu, L., Yin, M., Fu, L., Yang, F.: Uncertainty-aware pseudo-label and consistency for semi-supervised medical image segmentation. *Biomedical Signal Processing and Control* **79**, 104203 (2023)
12. Milletari, F., Navab, N., Ahmadi, S.A.: V-net: Fully convolutional neural networks for volumetric medical image segmentation. In: 2016 Fourth International Conference on 3D Vision (3DV). pp. 565–571. IEEE (2016)
13. Qi, W., Wu, H.C., Chan, S.C.: Mdf-net: A multi-scale dynamic fusion network for breast tumor segmentation of ultrasound images. *IEEE Transactions on Image Processing* **32**, 4842–4855 (2023)
14. Qi, W., Wu, J., Chan, S.C.: Gradient-aware for class-imbalanced semi-supervised medical image segmentation. In: European Conference on Computer Vision. pp. 473–490. Springer (2024)
15. Qiao, P., Li, H., Song, G., Han, H., Gao, Z., Tian, Y., Liang, Y., Li, X., Zhou, S.K., Chen, J.: Semi-supervised ct lesion segmentation using uncertainty-based data pairing and swapmix. *IEEE Transactions on Medical Imaging* **42**(5), 1546–1562 (2022)
16. Rizve, M.N., Duarte, K., Rawat, Y.S., Shah, M.: In defense of pseudo-labeling: An uncertainty-aware pseudo-label selection framework for semi-supervised learning. arXiv preprint arXiv:2101.06329 (2021)
17. Ronneberger, O., Fischer, P., Brox, T.: U-net: Convolutional networks for biomedical image segmentation. In: International Conference on Medical Image Computing and Computer-Assisted Intervention. pp. 234–241. Springer (2015)
18. Su, J., Luo, Z., Lian, S., Lin, D., Li, S.: Mutual learning with reliable pseudo label for semi-supervised medical image segmentation. *Medical Image Analysis* **94**, 103111 (2024)
19. Taghanaki, S.A., Zheng, Y., Zhou, S.K., Georgescu, B., Sharma, P., Xu, D., Comaniciu, D., Hamarneh, G.: Combo loss: Handling input and output imbalance in multi-organ segmentation. *Computerized Medical Imaging and Graphics* **75**, 24–33 (2019)
20. Tang, F., Xu, Z., Hu, M., Li, W., Xia, P., Zhong, Y., Wu, H., Su, J., Ge, Z.: Neighbor does matter: Density-aware contrastive learning for medical semi-supervised segmentation. *Proceedings of the AAAI Conference on Artificial Intelligence* **39**(7), 7220–7228 (Apr 2025). <https://doi.org/10.1609/aaai.v39i7.32776>, <https://ojs.aaai.org/index.php/AAAI/article/view/32776>
21. Tang, H., Chen, X., Liu, Y., Lu, Z., You, J., Yang, M., Yao, S., Zhao, G., Xu, Y., Chen, T., et al.: Clinically applicable deep learning framework for organs at risk delineation in ct images. *Nature Machine Intelligence* **1**(10), 480–491 (2019)
22. Wang, H., Li, X.: Dhc: Dual-debiased heterogeneous co-training framework for class-imbalanced semi-supervised medical image segmentation. In: International Conference on Medical Image Computing and Computer-Assisted Intervention. pp. 582–591. Springer (2023)
23. Wang, H., Li, X.: Towards generic semi-supervised framework for volumetric medical image segmentation. *Advances in Neural Information Processing Systems* **36**, 1833–1848 (2023)
24. Wu, Z., Shen, C., Hengel, A.v.d.: Bridging category-level and instance-level semantic image segmentation. arXiv preprint arXiv:1605.06885 (2016)

25. Xiang, J., Qiu, P., Yang, Y.: Fussnet: Fusing two sources of uncertainty for semi-supervised medical image segmentation. In: International Conference on Medical Image Computing and Computer-Assisted Intervention. pp. 481–491. Springer (2022)
26. Yao, H., Hu, X., Li, X.: Enhancing pseudo label quality for semi-supervised domain-generalized medical image segmentation. In: Proceedings of the AAAI Conference on Artificial Intelligence. vol. 36, pp. 3099–3107 (2022)
27. Yu, L., Wang, S., Li, X., Fu, C.W., Heng, P.A.: Uncertainty-aware self-ensembling model for semi-supervised 3d left atrium segmentation. In: International Conference on Medical Image Computing and Computer-Assisted Intervention. pp. 605–613. Springer (2019)
28. Zhong, Y., Luo, Z., Liu, C., Tang, F., Hu, Y., Peng, Z., Hu, M., Su, J., Ge, Z., Razzak, I.: Pg-sam: A fine-grained prior-guided sam framework for prompt-free medical image segmentation. In: 2025 IEEE International Conference on Bioinformatics and Biomedicine (BIBM). pp. 3369–3376 (2025). <https://doi.org/10.1109/BIBM66473.2025.11356599>